第 27 卷第 9 期
2011 年 9 月

无 机 化 学 学 报
CHINESE JOURNAL OF INORGANIC CHEMISTRY

Vol.27 No.9
1817-1829

# 阳离子和两性混合表面活性剂为模板合成三维六方介孔二氧化硅

张剑波[1] 杨宇翔*,[2] 郑九丽[2] 袁宏明[3] 曹 磊[2] 陈 诚[2]

([1]北京大学环境科学与工程学院,北京 10087)

([2]华东理工大学化学与分子工程学院,上海 200237)

([3]无机合成与制备化学国家重点实验室,吉林大学化学学院,长春 130012)

**摘要**:用阳离子表面活性剂 $C_n$TAB($n$=12,14,16,18)和两性生物表面活性剂 SDG 以 8:2 的摩尔比混合作为模板剂,在酸性条件下晶化,碱性条件下老化合成了三维有序介孔二氧化硅。合成的产物用 XRD、SEM、TEM 和 $N_2$ 吸附进行表征。结果表明,在不同链长的表面活性剂 $C_n$TAB($n$=12,14,16,18)中,$C_{14}$TAB 与 SDG 混合所得样品 $C_{14}$DG 的有序度最好。而 $C_{16}$TAB 和 $C_{18}$TAB 与 SDG 混合所得样品的孔径约为 9 nm。两性表面活性剂 SDG 对产物的形貌和三维六方结构都有影响。

**关键词**:介孔二氧化硅;两性表面活性剂 SDG;阳离子表面活性剂 $C_n$TMBr;三维六方

**中图分类号**:O613.72;O647.32 **文献标识码**:A **文章编号**:1001-4861(2011)09-1817-13

# Synthesis of Mesoporous Silica with a Three-Dimensional Hexagonal Ordered Structure Using Cationic and Amphoteric Mixed Surfactants

ZHANG Jian-Bo[1] YANG Yu-Xiang*,[2] ZHENG Jiu-Li[2] YUAN Hong-Ming[3] CAO Lei[2] CHEN Cheng[2]

([1]*Department of Environmental Sciences, Peking University, Beijing* 100871, *China*)

([2]*School of Chemistry and Molecular Engineering, East China University of Science & Technology, Shanghai* 200237, *China*)

([3]*State Key Laboratory of Inorganic Synthesis and Preparative Chemistry, College of Chemistry, Jilin University, Changchun* 130012, *China*)

**Abstract:** Ordered mesoporous silica with a 3D hexagonal structure was synthesized using mixed cationic $C_n$TMBr ($n$=12, 14, 16, 18) and amphoteric biological surfactants sodium N-dodecyl glycine (SDG) at a molar ratio of 8:2. Synthesis proceeded with hydrolysis and condensation of tetraethyl orthosilicate (TEOS) under acidic conditions, followed by aging in an alkaline medium. The synthesized products were characterized using X-ray diffraction, scanning electron microscopy, transmission electron microscopy, and nitrogen sorption analysis. Mesoporous silica with pore diameter of about 9 nm was obtained using $C_{16}$TMBr or $C_{18}$TMBr and SDG, as mixed templates. The presence of the amphoteric biological surfactant SDG was responsible for formation of the 3D hexagonal structure.

**Key words:** mesoporous silica; amphoteric surfactants SDG; cationic $C_n$TMBr; 3D hexagonal structure

## 0 Introduction

Mesoporous silica with various structures and morphologies has been synthesized using cationic surfactant cetyltrimethylammonium bromide ($C_{16}$TMBr) as a single template in a mixture of tetraethyl orthosilicate (TEOS) as a silica source under acidic conditions[1-4]. Compared to the single template system,

收稿日期:2011-01-25。收修改稿日期:2011-06-13。

国家自然科学基金(No.20971043 和 No.20577010)及吉林大学无机合成与制备化学国家重点实验室资助项目。

*通讯联系人。E-mail:yxyang@ecust.edu.cn

a mixed template system of two or more of the same or different types of surfactants has advantages such as variable critical micellar temperature (CMT) and critical micellar concentration (CMC) values, tuned pore sizes and pore structures, and phase transitions. Chen et al.[5] synthesized highly ordered mesoporous silica with a bicontinuous cubic structure using nonionic block copolymer and anionic mixed surfactants. Yeh et al.[6] synthesized hollow silica spheres with mesostructured shells using cationic-anionic-neutral block copolymer ternary surfactants. Taku et al.[7] prepared highly ordered mesoporous silica with a lamellar structure using an assembly of cationic and anionic surfactant mixtures as a template. Yang et al.[8] synthesized ordered mesoporous silica with the morphologies from spherical shape to rod-like and lamellar shape by using mixed surfactants, $C_{16}$TMBr and sodium dodecylsulfate.

To the best of our knowledge there have been no reports involving synthesis using cationic and amphoteric surfactant mixed templates. We report here the mesoporous silica synthesis by using mixed-surfactant templates $C_n$TMBr ($n$=12, 14, 16, 18) and amphoteric amino acid surfactant sodium N-dodecyl glycine (SDG). The molar ratio, chain length of the cationic surfactants, and synthesis conditions are discussed. Highly ordered mesoporous silica was prepared using acid crystallization and alkaline aging instead of the traditional acid synthesis route.

## 1 Experimental

### 1.1 Chemicals

Tetraethyl orthosilicate (TEOS, A.R.), Ammonia (A.R.) and Sulfuric acid (A.R.) were purchased from Sinopharm Chemical Reagent Co., Ltd. Dodecyltrimethyl ammonium bromide ($C_{12}$TMBr) (A.R.), tetradecyltrimethyl ammonium bromide ($C_{14}$TMBr) (A.R.), cetyltrimethyl ammonium bromide ($C_{16}$TMBr) (A.R.), and octadecyltrimethyl ammonium bromide ($C_{18}$TMBr) (A.R.) were obtained from Shanghai Lingfeng Chemical Reagent Co., Ltd. Sodium N-dodecyl glycine (SDG) (C.P.) was purchased from Shanghai Zhongshi Science and Technology Co., Ltd.

### 1.2 Synthesis of mesoporous silica

A typical synthesis was as follows: 1.5 g $C_{16}$TMBr and 0.2 g SDG dissolved in 67 mL deionized water, and 5 mL $H_2SO_4$ (98%, *w*/*w*) was added into the mixed surfactant solution at 30 ℃. The solutions were stirred for 1 h to completely dissolve the surfactants, and then 3.35 mL TEOS was added dropwise to the solution. After the mixture was stirred for 24 h, 12.5 mL $NH_3H_2O$ (25%, *w*/*w*) was added into the solution and stirred for 1 min, and the resulting mixture was aged at 80 ℃ for 24 h. The final reactant molar composition was $x$$C_{16}$TMBr:(1−$x$)SDG:18.7$H_2SO_4$:741 $H_2O$:3TEOS:47$NH_3H_2O$, and molar ratio of $C_{16}$TMBr/SDG [$x$/(1−$x$)] was named R for study on parallel synthesis of mesoporous silica using mixtures of cationic surfactants and SDG. The solid products were collected by filtration, washed with water, and dried in air at room temperature. The resultant powders were calcined at 550 ℃ for 6 h in air to remove the templates, and the final mesoporous silica materials were obtained.

Synthesis of other samples using various chain lengths of cationic surfactants ($C_n$TMBr, $n$=12, 14, 16, 18) was performed using the same procedure. The final reactant molar composition was 0.8$C_n$TMBr:0.2SDG:18.7$H_2SO_4$:741$H_2O$:3TEOS:47$NH_3\cdot H_2O$. The calcined products are referred to as $C_{12}$DG, $C_{14}$DG, $C_{16}$DG, and $C_{18}$DG according to their cationic surfactant chain length.

### 1.3 Characterization

The powder X-ray diffraction measurements of the mesoporous silica were performed on a D/max 2550 VB/PC X-ray diffractometer using Ni-filtered Cu $K\alpha$ radiation ($\lambda$=0.154 18 nm) [40 mA, 40 kV, 1°($2\theta$)·$min^{-1}$] at room temperature. High-resolution transmission electron microscopy (HRTEM) was performed with a JEOL JEM-2100 microscope operating at 200 kV (Cs), 0.6 mm with a resolution of 0.17 nm. The surface morphology of the mesoporous silica was observed using a Hitachi s4800 field emission scanning electron microscope with an accelerating voltage of 15.0 kV. Nitrogen adsorption/desorption isotherms were recorded using an ASAP2405 (Micromeritics Instrument Corp., Norcross, GA) physical adsorption apparatus. The

surface area was calculated using the Brunauer-Emmett-Teller (BET) method, and the pore size was obtained from the maxima of the pore-size distribution curves calculated using the Barrett-Joyner-Halenda (BJH) method with the adsorption branch of the isotherm.

## 2 Results and discussion

### 2.1 Synthesis of mesoporous silica using different processes

The synthesis conditions in the mixed-system using different processes were examined, including the process of acid crystallization followed by acid aging, alkaline crystallization followed by alkaline aging, and acid crystallization followed by alkaline aging. The low angle X-ray diffraction (LAXRD) patterns for the samples obtained using different processes are presented in Fig.1. As shown in Fig.1(a) and (b), when the mixture of $C_{16}$TMBr and SDG was used as a template, no ordered product was obtained in the process of alkaline crystallization followed by alkaline aging. Using the process of acid crystallization followed by acid aging, poorly ordered mesoporous silica was formed. The results were quite different from the products synthesized using $C_{16}$TMBr as a single template under acid or alkaline conditions[9]. Well ordered mesoporous silica was synthesized only in the process of acid crystallization followed by alkaline aging. A strong diffraction peak at about $2\theta$ =2.10° and two weak diffraction peaks at about $2\theta$ =3° ~5° are shown in Fig.1(c).

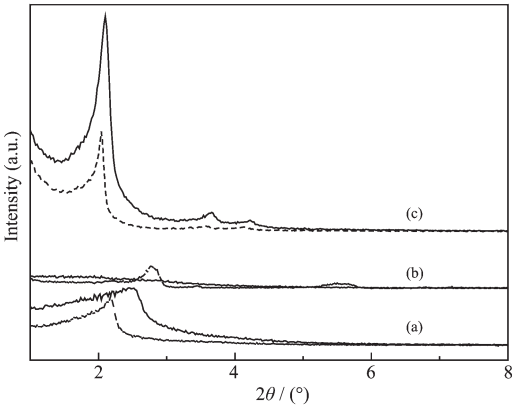


(a) Acid crystallization followed by acid aging, (b) Alkaline crystallization followed by alkaline aging, (c) Acid crystallization followed by alkaline aging; ---: As-synthesized, —: Calcined

Fig.1 LAXRD patterns of products formed under different pH values

According to Iler[10], as the pH value decreases and approaches to the point of zero charge(PZC) (pH=1.5~2.5), condensation of polysilicic acids becomes rate limiting, resulting in extremely long gelation times and very linear or cyclic oligomer of silica species in solution, due to a very small dissociation degree of polysilicic acids. At the same time, the adjacent SiOH groups on the linear or cyclic oligomer condense making further ring closures possible, thus leading to more compact, three-dimensional species. An increase in pH value or in the added amount of alkali is beneficial to three-dimensional species self-assembly to form an ordered structure through the surfactant-templating route[10]. Ordered mesoporous silica is shown in Fig.1(a) and (c). During the aging process, the addition of $NH_3H_2O$ transforms the interactions of the silica wall and surfactant from weak hydrogen bonding to a strong electrostatic interaction. The stronger electrostatic interactions induce the silica wall and surfactant to rearrange and restructure into a well ordered mesostructure[11]. As an amino acid amphoteric surfactant, SDG has amido and carboxyl groups in its molecular structure. The positive charge of hydrophilic cations is carried by amido groups, and the negative charge is carried by carboxyl groups. Thus, during the alkaline aging process, negatively charged $COO^-$ in SDG are expected to mutually combine with the cationic surfactant $CTA^+$ through electrostatic interactions, leading to a decrease in repulsion between head groups of the cationic surfactants, which causes the surfactants to arrange more closely in the micelles.

In the process of alkaline crystallization followed by alkaline aging, the electrostatic repulsion between silica species ($I^-$) and negatively charged $COO^-$ in the SDG of the mixed micelles accelerates the rate for condensation of the silicon species, resulting in the formation of disordered products, as shown in Fig.1(b).

### 2.2 Synthesis of mesoporous silica using mixtures of cationic surfactants and SDG with different mixing molar ratios

Mesoporous silica was synthesized using mixtures

of cationic surfactants and SDG with different molar ratios of $C_{16}$TMBr/SDG, R, in the process of acid crystallization followed by alkaline aging. The LAXRD patterns of mesoporous silica formed with different R values are shown in Fig.2. The results show that the ordered mesoporous silica products are obtained regardless of the molar ratio of $C_{16}$TMBr and SDG. An increase in the molar ratio of $C_{16}$TMBr to SDG improves the degree of order for the products. When R is 8:2, the highest ordered mesoporous silica is obtained.

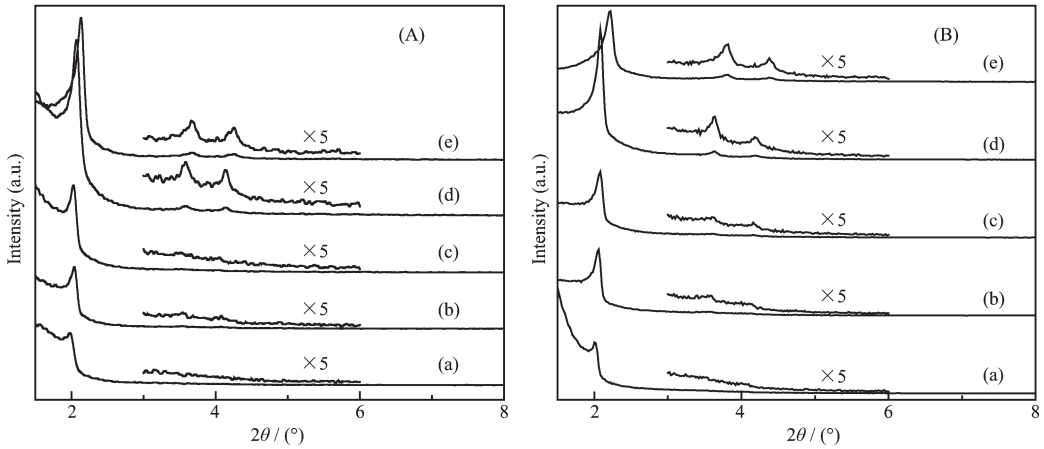


(a) $R$=5/5, (b) $R$=6/4, (c) $R$=7/3, (d) $R$=8/2, (e) $R$=9/1

Fig.2 LAXRD patterns of mesoporous silica formed using mixtures of cationic surfactants and SDG with different mixing molar ratios, $R$ (A: as-synthsized; B: calcined)

According to the LAXRD patterns, the synthesized products are with a hexagonal structure. The interplanar spacing, $d_{100}$, is calculated using the Bragg formula, $\lambda = 2d\sin\theta$, and the cell parameters, $a_0$, are calculated using the relationship $a_0=2d_{100}/3^{1/2}$, where $d_{100}$ is the interplanar spacing of the synthesized products after calcination.

LAXRD results are shown in Table 1, where the $\Delta d_{100}$ values show shrinkage of the cell after calcination due to template removal and silicate species polycondensation in the pore wall. Thus, when the silicate species polycondensation degree is high in the mesoporous material formation, a compact pore wall is formed, resulting in a decreasing $\Delta d_{100}$ value. As shown in Table 1, the highest ordered mesoporous silica has the smallest $\Delta d_{100}$ value, indicating that the molar ratio of 8:2 is the optimum value for obtaining the ordered mesoporous silica with a compact pore wall.

**Table 1 Physical properties of products with different Rs**

| $R$ | As-synthesized | | Calcined | | $\Delta d_{100}$ / nm |
|---|---|---|---|---|---|
| | $2\theta$ / (°) | $d_{100}$ / nm | $2\theta$ / (°) | $d_{100}$ / nm | |
| 5:5 | 1.98 | 4.46 | 2.01 | 4.39 | 0.07 |
| 6:4 | 2.03 | 4.34 | 2.06 | 4.29 | 0.05 |
| 7:3 | 2.04 | 4.33 | 2.08 | 4.24 | 0.09 |
| 8:2 | 2.07 | 4.26 | 2.09 | 4.22 | 0.04 |
| 9:1 | 2.12 | 4.16 | 2.20 | 4.01 | 0.15 |

## 2.3 Synthesis of mesoporous silica with different chain lengths of cationic surfactants

### 2.3.1 IR spectra

The IR spectra of the four calcined products synthesized using mixtures of SDG and cationic surfactants of different chain lengths are similar (Fig.3). The absorption bands around 3 340 $cm^{-1}$ are the characteristic absorptions of -OH bonds. The band at 1 630 $cm^{-1}$ is assigned to the H-O-H bending vibration. The sharp band of the asymmetric Si-O-Si stretching vibration is confirmed by the band at 1 085 $cm^{-1}$. The three bands at 962 $cm^{-1}$, 802 $cm^{-1}$, and 465 $cm^{-1}$ are

assigned to the Si-O stretching vibration. Moreover, no other IR peaks are seen in the spectra of the four calcined products, demonstrating that the samples are pure silica after calcination.

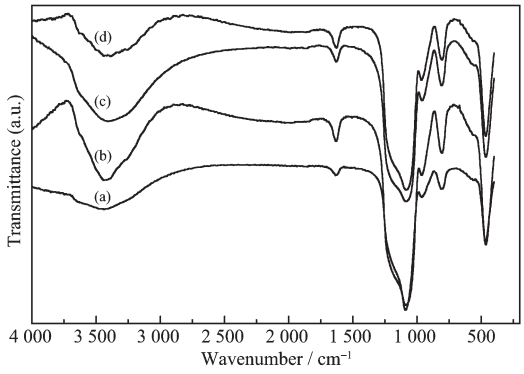


(a) $C_{12}$TMBr/SDG, (b) $C_{14}$TMBr/SDG, (c) $C_{16}$TMBr/SDG, (d) $C_{18}$TMBr/SDG

Fig.3　IR spectra of calcined samples synthesized using mixtures of SDG and cationic surfactants with different chain lengths

### 2.3.2　LAXRD

The LAXRD patterns of samples synthesized using mixtures of SDG and cationic surfactants $C_n$TMBr ($n$= 12, 14, 16, 18) with different hydrophobic chain lengths are shown in Fig.4. Except for the sample prepared in the mixed system $C_{12}$TMBr /SDG, all the samples show one strong diffraction peak, two weak diffraction peaks in the range of 3°~5°, and three well resolved peaks with a $1:\sqrt{3}:2$ interlamellar spacing ratio, demonstrating that the samples have a hexagonal structure. The calcined samples show higher peak heights than the as-synthesized samples, indicating calcination improves the degree order. The average pore wall thickness <$h$> was estimated by cellular model, using the equation[12], $h=2a_0\frac{(1-\varepsilon_{me})}{\varepsilon_{me}}\left(\frac{\zeta\varepsilon_{me}}{36\pi\gamma}\right)^{1/3}$, where $\varepsilon_{me}$ is the mesoporosity of the 3D hexagonal structure, $\zeta$ is isoperimetric quotient in the cellular model, $\gamma$ is number of cavities per unit cell in 3D hexagonal nanomaterials. The results are listed in the Table 2.

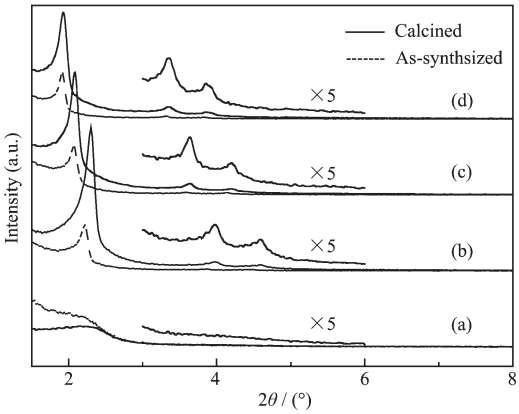


(a) $C_{12}$TMBr/SDG, (b) $C_{14}$TMBr/SDG, (c) $C_{16}$TMBr/SDG, (d) $C_{18}$TMBr/SDG

Fig.4　LAXRD patterns of samples formed using mixtures of SDG and cationic surfactants with different chain lengths

According to Table 2, the $\Delta d_{100}$ value decreases with increasing in hydrophobic chain length, corresponding to denser pore walls. Longer hydrophobic chain lengths correspond to larger $a_0$, pore diameter, surfactant area, pore volume of the products, and the larger average pore wall thickness <$h$>, with the exception of sample $C_{14}$DG. Moreover, sample $C_{14}$DG has the thinnest wall thickness of 0.463 nm, probably due to the largest shrinkage of the cell after calcination shown in Table 2.

The LAXRD data of samples formed using mixtures of SDG and cationic surfactants can be indexed; the results of indexing to the LAXRD pattern are given in Table 3. Table 3 shows that all the diffraction peaks in the pattern of samples $C_{14}$DG, $C_{16}$DG and $C_{18}$DG can be readily indexed by a set of lattice parameters. The largest relative deviation

**Table 2　Porous properties of samples formed using mixtures of SDG and cationic surfactants with different chain lengths**

| Sample | As-synthesized | | Calcined | | $\Delta d_{100}$ / nm | $a_0$ / nm | $S_{BET}$ / ($m^2\cdot g^{-1}$) | $V_P$ / ($cm^3\cdot g^{-1}$) | $D$ / nm | <$h$> / nm |
|---|---|---|---|---|---|---|---|---|---|---|
| | 2$\theta$ / (°) | $d_{100}$ / nm | 2$\theta$ / (°) | $d_{100}$ / nm | | | | | | |
| $C_{12}$DG | | | 2.18 | 4.05 | | 4.68 | 723.26 | 0.944 | 5.22 | 0.487 |
| $C_{14}$DG | 2.21 | 4.01 | 2.29 | 3.85 | 0.17 | 4.45 | 950.69 | 1.52 | 6.39 | 0.463 |
| $C_{16}$DG | 2.05 | 4.31 | 2.10 | 4.20 | 0.11 | 4.85 | 758.14 | 1.687 | 8.91 | 0.505 |
| $C_{18}$DG | 1.91 | 4.62 | 1.93 | 4.57 | 0.05 | 5.28 | 1 032.09 | 2.355 | 9.13 | 0.550 |

**Table 3 Results of indexing to LAXRD of samples formed using mixtures of SDG and cationic surfactants with different chain lengths**

| | Hexagonal symmetry $a$=3.853 $c$=2.602 nm ($c$ may be taken arbitrary value by calculation) | | | | |
|---|---|---|---|---|---|
| $C_{14}$DG Sample b | 2$\theta$ / (°) | $D_{exp}$ / nm | $D_{cal}$ / nm | $hkl$ | $I$ / % |
| | 2.292 | 3.851 6 | 3.853 2 | 100 | −0.016 |
| | 3.967 | 2.225 3 | 2.224 6 | 110 | 0.006 5 |
| | 4.576 | 1.929 2 | 1.926 6 | 200 | −0.026 |
| | Hexagonal symmetry $a$=4.227 $c$=2.700 nm ($c$ may be taken arbitrary value by calculation) | | | | |
| $C_{16}$DG Sample c | 2$\theta$ / (°) | $D_{exp}$ / nm | $D_{cal}$ / nm | $hkl$ | $I$ / % |
| | 2.089 | 4.226 0 | 4.222 0 | 100 | 0.039 |
| | 3.628 | 2.433 1 | 2.437 6 | 110 | −0.045 |
| | 4.187 | 2.108 5 | 2.111 0 | 200 | −0.025 |
| | Hexagonal symmetry $a$=4.570 $c$=2.820 nm ($c$ may be taken arbitrary value by calculation) | | | | |
| $C_{18}$DG Sample d | 2$\theta$ / (°) | $D_{exp}$ / nm | $D_{cal}$ / nm | $hkl$ | $I$ / % |
| | 1.929 | 4.576 0 | 4.569 9 | 100 | 0.061 4 |
| | 3.358 | 2.628 9 | 2.638 4 | 110 | −0.095 |
| | 3.865 | 2.284 0 | 2.285 0 | 200 | −0.010 |

between the calculated and experimental is 0.049%, 0.21% and 0.64% for samples $C_{14}$DG, $C_{16}$DG and $C_{18}$DG, respectively, which indicates that the samples $C_{14}$DG, $C_{16}$DG and $C_{18}$DG are all a single phase with a hexagonal symmetry.

But a set of lattice parameters for the samples is obtained in the absence of b value, as can be seen from Table 3, because a is equal to b in the hexagonal phase. It is also found that the c value has no influence on the calculated results in the calculation process. It is possible that the c axis corresponds to the direction of a long parallel-arranged pore channel, and its length may be different with different surfactant chain lengths[13].

According to the principle of hydrophilic-hydrophobic balance (HLB)[14], during the process of micelle self-assembly, the hydrophilic and the hydrophobic parts of the surfactant need to remain balanced. Because the same types of cationic surfactants ($C_n$TMBr) have the same effective head group, an increase in hydrophobic chain length would cause the HLB to shift to the hydrophobic side. Thus, more counterion association is required to maintain balance with an increased hydrophobic chain length. Therefore, more silicate species are catalyzed and condensed on the micellar surface in the same reaction time, resulting in denser pore walls. Thus, the product has thicker pore walls and less shrinkage of the cell after calcination.

Fig.4 shows that sample $C_{14}$DG has the highest degree of order among the four samples. Because the two surfactants $C_{14}$TMBr and SDG have the same hydrophobic chain length, when they are mixed, the molecular packing at the air/water interface is closer. However, when the chain length for the two surfactants $C_n$TMBr and SDG is different, the portion of the molecules above the height of the adjacent molecules exhibits thermal motion. The thermal disturbance presumably propagates along the chain at a considerable length towards the polar group of the molecule, leading to an increase in the area/molecule for higher-length chain molecules. Thus, when cationic and amphoteric surfactants form mixed micelles, their different chain lengths result in a looser-packed micelle and a decrease in the degree of order in the products[15].

2.3.3 Nitrogen adsorption/desorption measurements

The $N_2$ sorption isotherms of the products formed using mixtures of different chain length cationic surfactants and the amphoteric surfactant SDG as a template (molar ratio 8:2) are shown in Fig.5. All samples show the characteristic type Ⅳ reversible $N_2$ sorption isotherm described for typical mesoporous materials. Adsorption isotherms of all the products show three well distinguished regions: mono- and multilayer adsorption on the pore walls, capillary condensation,

and multilayer adsorption on the outer surface. Within the relative pressure range from the middle to near saturation, the adsorption isotherms all have a $H_1$ hysteresis loop in which the hysteresis loop is narrow, and the adsorption and desorption branches are nearly vertical and parallel. The results show that the products have a mesoporous structure and cylindrical channels with uniform pore size and regular shape.

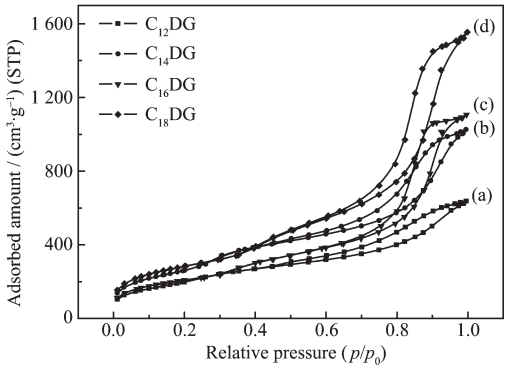


(a) $C_{12}$TMBr/SDG, (b) $C_{14}$TMBr/SDG, (c) $C_{16}$TMBr/SDG, (d) $C_{18}$TMBr/SDG

Fig.5　Nitrogen adsorption/desorption isotherms of the calcined samples synthesized using mixtures of SDG and cationic surfactants with different chain lengths

The position of the midrange of $p/p_0$ is generally accepted to be used as an important reference for judging pore size. The steep slope of the desorption branch and the adsorption branch can confirm the homogeneity of the pore size distribution. For higher $p/p_0$ values, the capillary condensation occurs with a larger hysteresis loop area, so the product has a larger pore size. As shown in Fig.5, an abrupt increase for the products $C_{12}$DG, $C_{14}$DG, $C_{16}$DG, and $C_{18}$DG is observed at $p/p_0 \approx 0.445$, $p/p_0 \approx 0.448$, $p/p_0 \approx 0.548$, and $p/p_0 \approx 0.55$, respectively. The product formed using mixtures of $C_{18}$TMBr and SDG, (d), shows the largest hysteresis loop area and the steepest slope; product (c) is the second and product (b) is the third, while the product formed using mixtures of $C_{12}$TMBr and SDG, (a), shows the smallest hysteresis loop area and the least steep slope. According to Fig.5, we conclude that as the hydrophobic chain length of the cationic surfactant increases, the pore size becomes larger and the pore size distribution becomes narrower.

Fig.6 shows the pore size distributions of samples $C_{12}$DG, $C_{14}$DG, $C_{16}$DG, and $C_{18}$DG determined using the KJS-modified BJH method. All the samples show apparent multi-peak distributions for pore size. For example, sample $C_{12}$DG shows a tri-peak distribution for pore sizes within the ranges of 1.98 ~3.00 nm, 3.00 ~4.33 nm, and 4.33 ~40.36 nm, which accounts for 33.93%, 16.25%, and 49.81% of the entire pore distribution, respectively. Sample $C_{14}$DG also shows a tri-peak distribution for pore sizes within the ranges of 1.89 ~2.98 nm, 3.33 ~4.19 nm, and 4.19 ~22.53 nm, which accounts for 21.55%, 14.57%, and 61.63% of the entire pore distribution, respectively. However, sample $C_{16}$DG shows a bi-peak distribution in the ranges of 1.83~5.22 nm and 5.22~21.86 nm, which accounts for 29.01% and 70.02% of the entire pore distribution, respectively. Similarly, the pore size of sample $C_{18}$DG shows a bi-peak distribution in the ranges of 1.84~5.24 nm and 5.24 ~23.31 nm, which accounts for 30.12% and 68.22% of the entire pore distribution, respectively. The mean pore sizes of samples $C_{12}$DG, $C_{14}$DG, $C_{16}$DG, and $C_{18}$DG are calculated to be 5.22 nm, 6.39 nm, 8.91 nm, and 9.13 nm, respectively.

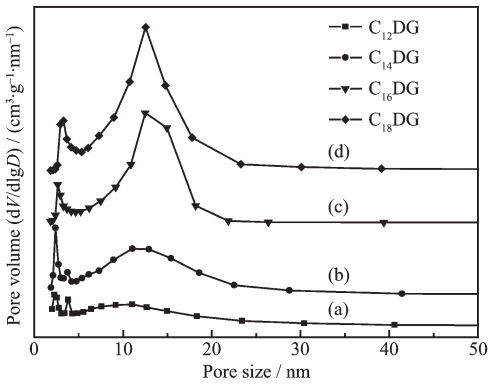


(a) $C_{12}$TMBr/SDG, (b) $C_{14}$TMBr/SDG, (c) $C_{16}$TMBr/SDG, (d) $C_{18}$TMBr/SDG

Fig.6　Pore size distribution of the calcined samples synthesized using mixtures of SDG and cationic surfactants with different chain lengths

According to the analysis above, as the hydrophobic chain lengths of cationic surfactants increase, the pore size of the samples increases. This is in good agreement with the previous XRD analysis. The multi-peak pore distributions are related to the 3D

hexagonal structure with interconnected channels[16]. In contrast to previous XRD analysis, the cell parameters ($a_o$) for samples $C_{12}DG$, $C_{14}DG$, $C_{16}DG$, and $C_{18}DG$ are all smaller than their mean pore size, demonstrating that the products have interconnected channels[16].

2.3.4 $\alpha_s$-Plot method

To confirm the formation of a micropore structure in $C_{12}DG$, $C_{14}DG$, $C_{16}DG$, and $C_{18}DG$ products, the $\alpha_s$-plot method was adopted[17]. This method is based on a comparison of the adsorption isotherm for a given porous material with adsorption data for a reference macroporous solid. For such $\alpha_s$-plot calculations[18], the macroporous silica gel LiChrospher Si-1000 ($S_{BET}$=25 $m^2 \cdot g^{-1}$) is used as the reference adsorbent. Note that the standard reduced adsorption is defined as $\alpha_s=v_{ref}(P/P_0)/v_{ref}$ (0.4), where $v_{ref}$ ($P/P_0$) and $v_{ref}$ (0.4) are the amount adsorbed onto the reference solid as a function of relative pressure and the amount adsorbed at a relative pressure of 0.4, respectively. A high-resolution $\alpha_s$-plot for the $C_{12}DG$, $C_{14}DG$, $C_{16}DG$, and $C_{18}DG$ products is constructed with $\alpha_s$ as the abscissa and the "volume adsorbed" for the sample as the ordinate. As illustrated in Fig.7, all the initial portions of the plots for the $C_{14}DG$, $C_{16}DG$, and $C_{18}DG$ products show a deviation from a straight line, with the curves commencing slightly above the origin of the graph, such behaviour most likely arises from the presence of detectable amounts of micropores, with non-uniform pore size distribution. But the $C_{12}DG$ product shows different from $C_{14}DG$, $C_{16}DG$, and $C_{18}DG$ products, the initial portion of its plot is virtually linear with the "volume adsorbed" curves commencing slightly above the origin of the graph, which demonstrates the $C_{12}DG$ product has small amount of micropores. When $\alpha_s$ is in the range from *ca.* 2.5 to 3.0, the amount adsorbed increases sharply. Finally, when the value of $\alpha_s$ is above 3.0, although the amounts adsorbed onto products $C_{14}DG$, $C_{16}DG$, and $C_{18}DG$ products continue to increase they do so more smoothly as the $\alpha_s$-value increases.

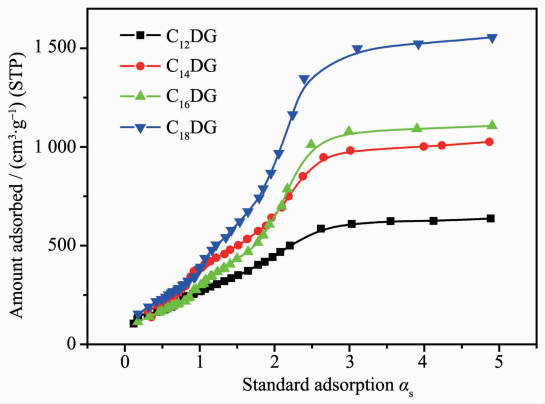


Fig.7 High-resolution $\alpha_s$-plots for the $C_{12}DG$, $C_{14}DG$, $C_{16}DG$, and $C_{18}DG$ products

With increasing surfactant chain length of cationic surfactant $C_nTMBr$, the micropore volume of the products $C_{12}DG$, $C_{14}DG$, $C_{16}DG$ and $C_{18}DG$ is 0.944, 1.52, 1.687 and 2.355 (Table 2), respectively, demonstrating that the micropores inside the pore wall of mesopore are adjustable. From Table 2, we also know though pore size of the main channel increases with increasing in hydrophobic chain length, the extent of the unit cell shrinkage during calcination decreases, leading to a slight increase of the pore wall thickness.

According to XU Ru-Ren[19], the micropores inside the pore wall can be expanded to small mesopores with increasing in hydrophobic chain length, and the small mesopores may connect main pore channel to form 3D mesoporous channel, but still maintaining their hexagonal symmetry, as can be seen in the following Fig.8. From Table 2, one can see the average pore size of samples formed using mixtures of SDG and cationic surfactants with different chain lengths are all higher than that of the corresponding 2D mesoporous channel using single cationic surfactants (such as $C_{14}TMBr$, $C_{16}TMBr$ and $C_{18}TMBr$)[13], but the former has thinner pore wall, chiefly due to expansion of micropores into mesopores, which leads to pore wall thickness becoming thinner.

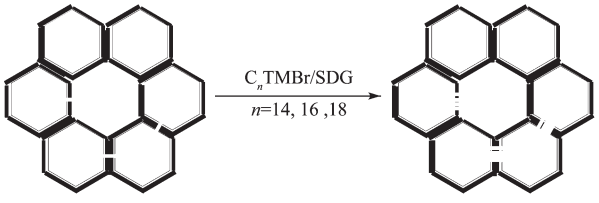


Fig.8 Schematic drawing of formation of 3D mesoporous channel

When the mixture of SDG and $C_{12}TMBr$ is used as template, the micropores inside the pore wall can not be

expanded to small mesopores, because the very short hydrophobic chain of $C_{12}$TMBr cannot take the route of a template under the experiment condition[13], leading to main pore channel being not connected. Moreover, the diffraction pattern of $C_{12}$DG product only displays a broad and undefined peak at 2.18° (Fig.4), indicating the sample formed using mixtures of SDG and $C_{12}$DG has a poor hexagonal order.

2.3.4　SEM

Fig.9(a), (c), (e), and (g) show the SEM images for

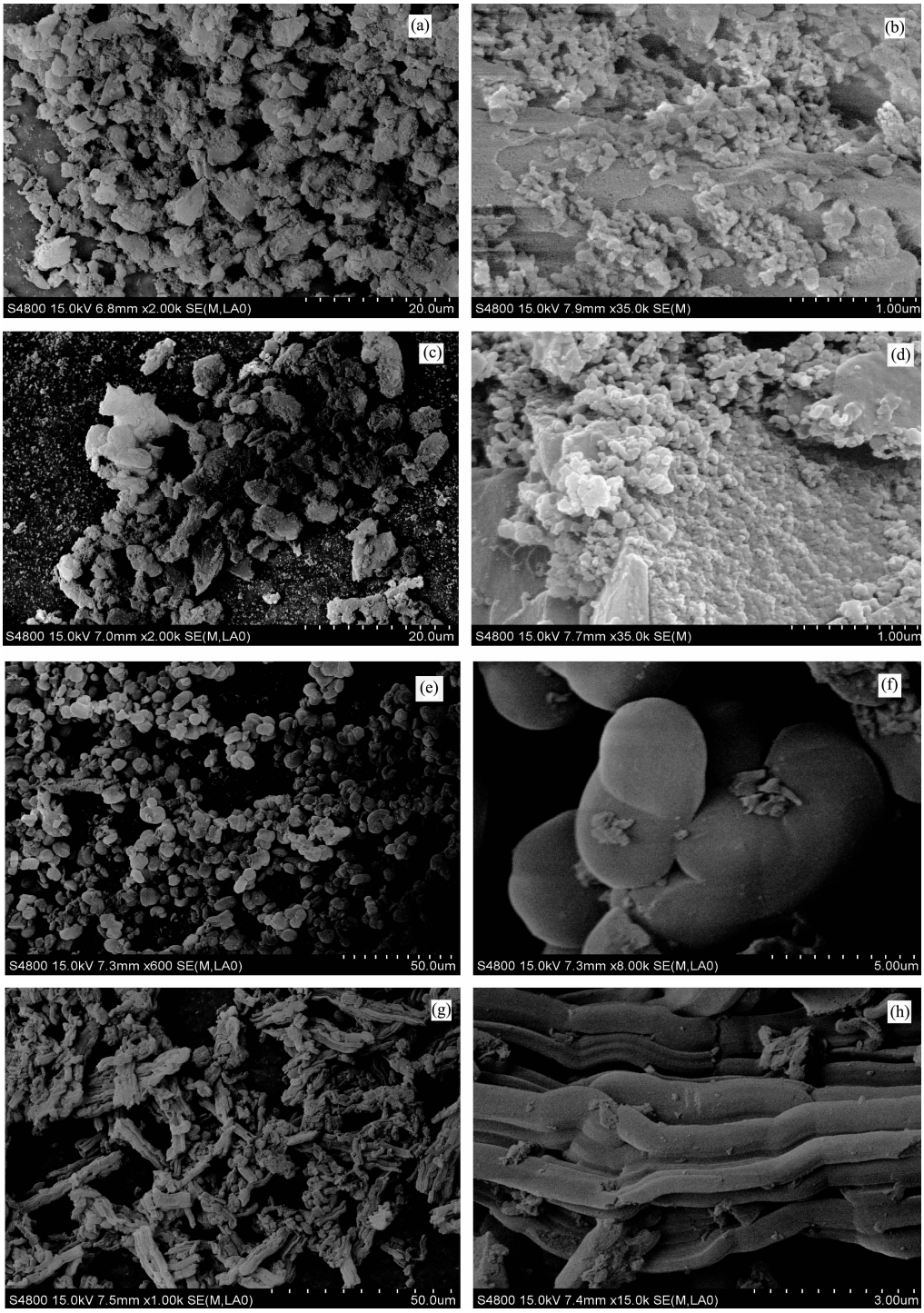


(a) $C_{12}$TMBr/SDG, (b) enlarged portion of Fig.9(a), (c) $C_{14}$TMBr/SDG, (d) enlarged portion of Fig.9(c), (e) $C_{16}$TMBr/SDG, (f) enlarged portion of Fig.9(e), (g) $C_{18}$TMBr/SDG, (h) enlarged portion of Fig.9(g)

Fig.9　SEM images for the calcined samples synthesized using mixtures of cationic surfactants and SDG as a template

the calcined products synthesized using mixtures of different chain length cationic surfactants and SDG as a template, while Fig.9(b), (d), (f), and (h) show enlarged portions of Fig.9(a), (c), (e), and (g), respectively.

Sample $C_{12}$DG shows a disordered blocklike structure [Fig.9(a)], in which the surface is covered with a small amount of aggregated, nonuniform spherical particles [Fig.9(b)]. Unlike sample $C_{12}$DG, sample $C_{14}$DG shows a mixture of bean-like and blocklike structures. Compared to $C_{12}$DG, an enlarged portion of $C_{14}$DG in Fig. 9(d) shows aggregates of spherical particles with a narrow distributed size.

Sample $C_{16}$DG shows primarily bean-like particles, accompanied by a small amount of spherical particles. Fig.9(f) is an enlarged portion of $C_{16}$DG, showing bean-like particles. Sample $C_{18}$DG has a characteristic rodlike structure, as shown in Fig.9(h), resulting from a piled-up mass with lamellar structure.

To explain the reason for the different morphological structure formation, we consider the surfactant packing parameter, g. The parameter g has been used as a guideline to predict and interpret the structures of products[20]. According to packing parameter requirements, the relationship $g=V_c/(l_c a_0)$ determines the shape of the micelles; when $g<1/3$, the surfactant aggregates in the form of a spherical micelle, $1/3<g<1/2$ results in a cylindrical micelle, and $1/2<g<1$ gives a flexible lamellar phase. The cationic surfactants used in the synthesis experiments are $C_{12}$TMBr, $C_{14}$TMBr, $C_{16}$TMBr, and $C_{18}$TMBr. As reported by Yang et al.[13], a longer hydro-phobic chain of cationic surfactants favors larger g values for these cationic surfactants.

Another factor is the amido groups in the molecular structure of the amphoteric biological surfactant SDG, which may have carried the positive charge of hydrophilic cations to form the cationic amino group[21]. For this reason, electrostatic repulsion occurs between the cationic amino groups and the adjacent array of cationic surfactant hydrophobic chains in the mixed-template reactions, including mixtures of cationic surfactants and SDG. When the array gap distance between SDG and the cationic surfactants is increased, the hydrophobic chains of the cationic surfactants become to curl up at a specific degree. As the hydrophobic surfactant chain length increases from $C_{12}$ to $C_{18}$, the corresponding degree of curling gradually increases. This will result in an increased molecular volume, and thus, the packing parameter, g, increases accordingly.

The third factor is that the effective head group is the same for different chain surfactants of the same type, $C_n$TMBr. Thus, a longer hydrophobic hydrocarbon chain makes the the hydrophilic-hydrophobic balance (HLB) shift to the hydrophobic side. The longer chain length results in a higher association constant for counterions, and thus, formation of longer rod micelles is favored[13,22].

Therefore we conclude that the long hydrophobic chain, electrostatic repulsion between amphoteric and cationic surfactants, and the increased degree of curling all lead to an increase in the packing parameter, g. Thus, two transitions, spherical to bean-like and bean-like to a lamellar structure, are involved lamellar structures formation from the self-assembly of micelles of the mixed-template $C_n$TMBr-SDG.

2.3.5 TEM

Fig.10 shows the HRTEM images of the calcined products synthesized using mixtures of cationic surfactants and SDG as templates. Regardless of the chain length of the cationic surfactant, 3D hexagonally structured mesoporous silica is formed in the different mixed systems of $C_n$TMBr-SDG. As shown in Fig.10(a), (c) and (e), structural alternation of pores and channels in different directions occurs. The circles indicate that samples $C_{12}$DG, $C_{14}$DG and $C_{18}$DG all have a 1D pore structure, but the arrowheads show that the 1D pores link with each other to form secondary channels, although the interconnections of the channels are short and discontinuous. The channels are linked in a random manner, but the phenomenon of cross-channels does not appear. Sample $C_{16}$DG has a 3D hexagonal structure, as shown in Fig.10 (b). As the direction of crystal growth changes during synthesis, a disconnected, ordered pore structure is formed [Fig.10 (b)]. The arrowheads show the change in direction of the crystal face. The distance between two pore centers for

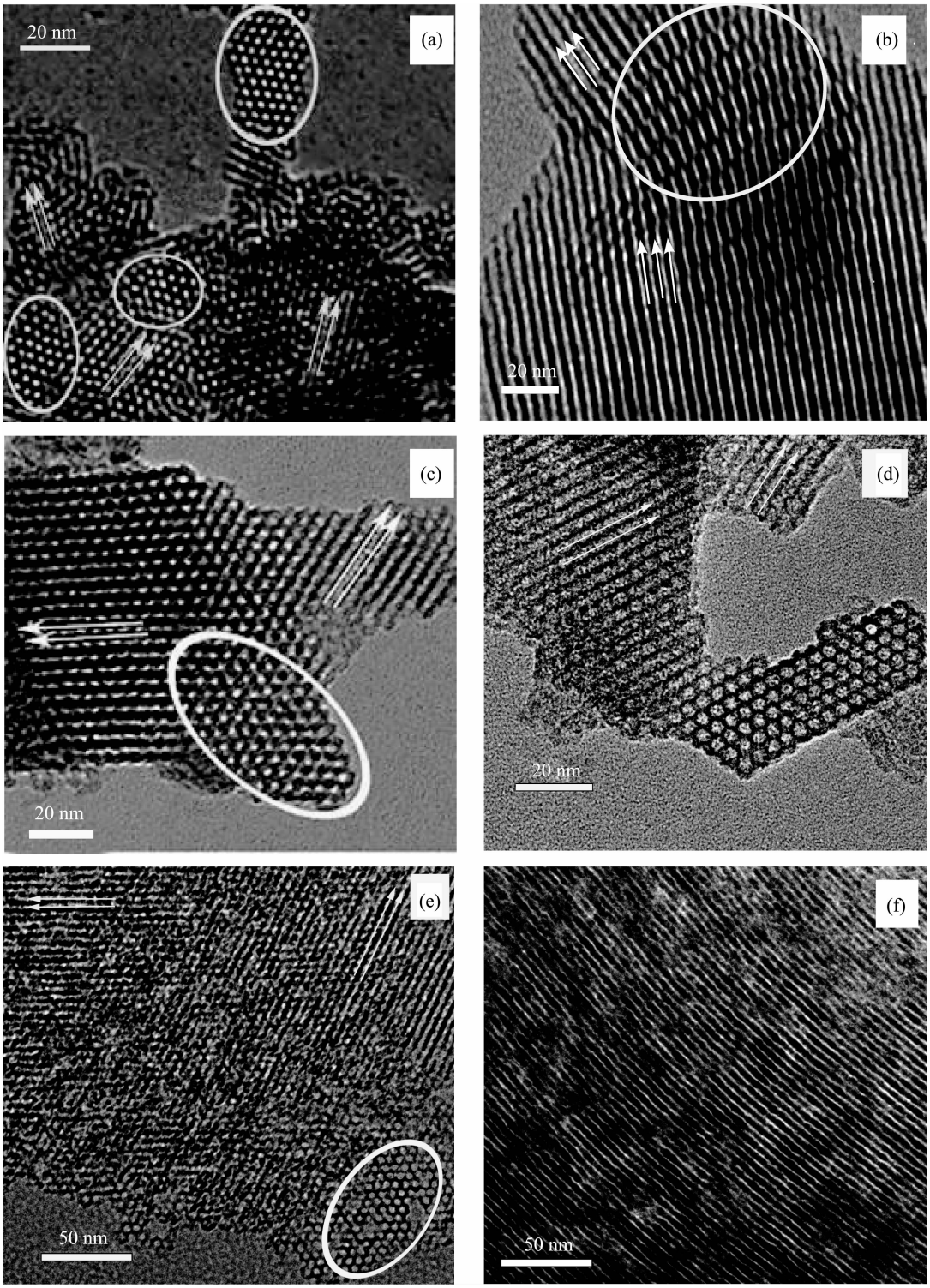


(a) $C_{12}$TMBr/SDG, (b) $C_{16}$TMBr/SDG, (c) $C_{14}$TMBr/SDG, (d) $C_{14}$TMBr/SDG, (e) $C_{18}$TMBr/SDG, (f) $C_{18}$TMBr/SDG

Fig.10　TEM images of the calcined samples formed using mixtures of cationic surfactants and SDG as templates

parallel pore channels is estimated to be 4.53 nm from the TEM image. The value is in good agreement with the value $a_0$=4.85 nm calculated from LAXRD.

Sample $C_{14}$DG has a 3D hexagonal structure, as shown in Fig.10(d). Two connected perpendicular channels, are arranged along [110] and [100] direction respectively. The top left hand corner of Fig.10(d) is TEM image recorded in [110] direction, the image

clearly shows ordered parallel arranged pore channel structure, the distance between two pore center is estimated as 4.59 nm from TEM images, the value is in good agreement with the value calculated from XRD data ($a_0$ calcd. value is 4.45 nm for $C_{14}$DG). The TEM image recorded in the lower right corner of Fig.10(d) can be indexed as [100] direction according to the results of XRD, the image clearly shows ordered hexagon mesostructure with ordered homogeneous pores hexagonal arranged.

Fig.10(f) is the TEM image of sample $C_{18}$DG recorded along the [110] direction, the image clearly shows ordered parallel arranged pore channel structure, the distance between two pore center is estimated as 5.13 nm from TEM images, it is in good agreement with the value calculated from XRD data ($a_0$ calcd. value is 5.28 nm).

2.3.6 Synthesis mechanism

Equation (**1**) is the ionization equilibrium equation of sodium N-dodecyl glycine SDG, where glycine belongs to the neutral amino acid and its isoelectric point is 5.97[23]. According to the ionization-equilibrium equation, amphoteric surfactant SDG is protonated and positively charged under acidic conditions (pH<1). In contrast, it is deprotonated and negatively charged under basic conditions (pH >11). Under pH value conditions between 1 and 11, amphoteric surfactant SDG exists in solution in a zwitterionic form.

In general, long-chain amphoterics that exist in solution in a zwitterionic form are more surface active than ionic surfactants with the same hydrophobic group[24] because the oppositely charged ions are neutralized. In this study, the pH value range is controlled at 2 ~8, and surfactant SDG exists in solution in a zwitterionic form, which can carry both positive charges and negative charges. Equation (**2**) shows bonding between SDG and CTAB, negatively charged carboxyl ($COO^-$) groups in SDG contacts $CTA^+$ to form the mixed micelles through electrostatic interactions.

$$C_{12}H_{25}\text{-}\overset{+}{N}H_2\text{-}CH_2\text{-}COOH \underset{H^+}{\overset{OH^-}{\rightleftharpoons}} C_{12}H_{25}\text{-}\overset{+}{N}H_2\text{-}CH_2\text{-}COO^- \underset{H^+}{\overset{OH^-}{\rightleftharpoons}} C_{12}H_{25}\text{-}NH\text{-}CH_2\text{-}COO^- \quad (1)$$

$$C_{12}H_{25}\text{-}\overset{+}{N}H_2\text{-}CH_2\text{-}COO^- + CTA^+B^- \underset{H^+}{\overset{OH^-}{\rightleftharpoons}} C_{12}H_{25}\text{-}\overset{+}{N}H_2\text{-}CH_2\text{-}COO^-CTA^+ + Br^- \quad (2)$$

For the mixed $C_n$TMBr/SDG system, the synthesis mechanism of mesoporous silica follows the $M^+X^-I^+$ route under acidic conditions. $I^+$ and $M^+$ are inorganic precursor cations and mixed surfactant micelles, respectively. $X^-$ represents halogen ions ($Cl^-$, $Br^-$, and $I^-$), $SO_4^{2-}$, and $NO_3^-$, among others. As shown in Fig.11, the mixed micelles are formed when SDG contacts CTAB through electrostatic interactions. The positive charges on the mixed micelles associate with the counterions ($X^-$) to form $M^+X^-$ micelle under acidic conditions, which catalyzes silicate precursors through hydrolysis and transforms into a sol of silicate oligomers. Through the interaction between inorganic counterions and mixed surfactant micelles, the silicate oligomers continue to concentrate on the micellar surface and eventually form silica micelles.

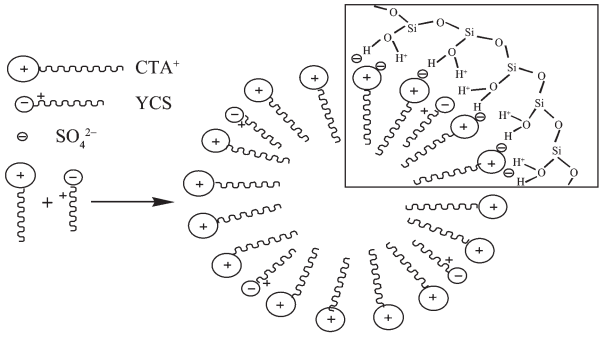


Fig.11 Schematic illustration of the synthesis mechanism

In the mixed micellar system, negatively charged carboxyl ($COO^-$) groups in SDG combine with $CTA^+$ through electrostatic interactions and decrease the number of positive charges. On the other hand, the presence of negative charges in the synthesis system causes repulsive electrostatic interactions, resulting in decreased bonding forces between the inorganic counterions and cationic surfactants in the synthesis system.

The association constant of the divalent $SO_4^{2-}$ is small[25] because the highly hydrated species $HSO_4^-$ is weakly bound to the surfactant. The weaker binding

force between the micelles and silicate species reduces the amount of silicate oligomer aggregates on the micellar surface, leading to the formation of a thinner pore wall. During the calcination process, the pore wall collapses to form the interconnected channels, inducing the formation of a hexagonal structure.

## 3 Conclusions

In the $C_{16}$TMBr-SDG mixed system, highly ordered mesoporous silica is formed when the molar ratio of $C_{16}$TMBr and SDG is 8:2 using acid crystallization followed by alkaline aging.

When mixing the cationic surfactants of different chain lengths ($C_n$TMBr, $n$=12, 14, 16, 18) with SDG, the sample $C_{14}$DG shows the highest degree of order. All the products have a 3D hexagonal structure. As the hydrophobic chain length increases, the morphologies of the products change from blocklike structures to bean-like structures, and then to rodlike structures.

The amphoteric biological surfactant SDG influences both the morphology and the 3D hexagonal structure of the products.

**Acknowledgements:** The authors are grateful to the financial support from National Natural Science Foundation of China (Grant No. 20971043, No. 20577010), and also grateful to Mr. LIU Xiang-Nong, Analysis & Testing Center, Yangzhou University for help in sample characterization.

## References:

[1] Monnier A, Schuth F, Huo Q, et al. *Science*, **1993**,**261**(5126):1299-1303

[2] Zhang J Y, Luz Z, Goldfarb D E. *J. Phys. Chem. B*, **1997**,**101**(36):7087-7094

[3] Lin H P, Mou C Y, Liu S B. *Adv. Mater.*, **2000**,**12**(2):103-106

[4] Lin H P, Liu S B, Mou C Y, et al. *Chem. Commun.*, **1999**:583-584

[5] Chen D H, Li Z, Yu C Z, et al. *Chem. Mater.*, **2005**,**17**(12):3228-3234

[6] Yeh Y Q, Chen B C, Lin H P, et al. *Langmuir*, **2006**,**22**(1):6-9

[7] Taku O, Kenichi S, Masahiko A, et al. *J. Phys. Chem. C*, **2008**, **112**(32):12184-12187

[8] Cao L, Shao J G, Yang Y B, et al. *Glass Phy. Chem.*, **2010**, **36**(2):182-189

[9] Beck J S, Vartuli J C, Kresge C T, et al. *J. Am. Chem. Soc.*, **1992**,**114**(27):10834-10843

[10]Iler R K, Editor. *The Chemistry of Silica*: *Solubility, Polymerization, Colloid and Surface Properties, and Biochemistry*. New York: John Wiley & Sons, **1979**:186,188,634,671,667-707

[11]Lin H P, Kuo C L, Wanb B Z , et al. *J. Chinese Chem. Soc.*, **2002**,**49**(5):899-906

[12]Ravikovitch P I, Neimark A V. *Langmuir*, **2002**,**18**(5):1550-1560

[13]Yang Y X, Ying H P, Shao J G, et al. *J. Am. Ceram. Soc.*, **2007**,**90**(11):3460-3467

[14]Lin H P, Mou C Y. *Acc. Chem. Res.*, **2002**,**35**(11):927-935

[15]Patist V, Chhabra R, Shah D, et al. *Langmuir*, **1997**,**13**(3):432-434

[16]Fan J, Yu C Z, Terasaki O, et al. *J. Am. Chem. Soc.*, **2001**, **123**(48):12113-12114

[17]Kruk M, Jaroniec M. *Langmuir*, **1997**,**13**(23):6267-6273

[18]Kruk M, Antochshuk V, Jaroniec M. *J. Phys. Chem. B*, **1999**, **103**(48):10670-10678

[19]XU Ru-Ren, PANG Wen-Qin, YU Ji-Hong, et al. *Chemistry-Zeolites and Porous Materials*. Beijing: Science Press, **2004**.

[20]Huo Q S, Margolese D I, Stucky G D, et al. *Chem. Mater.*, **1994**,**6**(8):1176-1191

[21]Yang Y X, Huang Z, Deng W J, et al. *Microporous Mesoporous Mater.*, **2008**,**116**:267-276

[22]Lin H P, Cheng Y R, Mou C Y. *Phys. Chem.*, **1999**,**1**:5051-5058

[23]Gao H-b. *Organic Chemistry*. China Higher Education Press (third edition). Beijing, **2004**:504

[24]Effendy I, Maibach H I. *Contact Dermatit*, **1995**,**33**:217-225

[25]Yang H, Vovk G, Ozin G A, et al. *Mater. Chem.*, **1998**,**8**(3):743-750